# Supporting information

## Ultrathin core-shell Au@RuNi nanowires for superior electrocatalytic hydrogen evolution†

*Xian Jiang,[a,b] Xianzi Wei,[a] Mushun Chen,[a] Chuankai Fu,[a] Yufei Wang,[b] Caikang Wang,[a,d] Hao Sun,*[c] Juan Zhou*[a,d] and Yawen Tang*[b]*

[a] School of New Energy, Nanjing University of Science and Technology, Jiangyin, 214443, China.

[b] Jiangsu Key Laboratory of New Power Batteries, Jiangsu Collaborative Innovation Centre of Biomedical Functional Materials, School of Chemistry and Materials Science, Nanjing Normal University, Nanjing 210023, China.

[c] Key Lab of Biomass Energy and Material, Jiangsu Province, Institute of Chemical Industry of Forest Products, Chinese Academy of Forestry, No. 16 Suojin 5th Village, Nanjing 210042, China.

[d] School of Energy and Power Engineering, Nanjing University of Science and Technology, 200 Xiaolingwei Street, Jiangsu Province, 210094, China.

**Corresponding Author**

E-mail address: 15850534739@163.com (H. Sun); jzhou@njust.edu.cn (J. Zhou); tangyawen@njnu.edu.cn (Y. Tang)

## Part I: Experimental

**Chemicals and Reagents:** 1-naphthol ($C_{10}H_8O$) was purchased from Aladdin (Shanghai, China). Hydrogen tetrachloroaurate (III) trihydrate ($HAuCl_4 \cdot 4H_2O$), ruthenium acetylacetonate ($Ru(acac)_3$), and nickel acetylacetonate ($Ni(acac)_2$) were supplied by Shanghai D&B Biological Science and Technology Co., Ltd. Polyvinylpyrrolidone (PVP), L-ascorbic acid (AA), ethylene glycol (EG), sodium hydroxide (KOH) and ethanol ($C_2H_5OH$) were purchased from Sinopharm Chemical Reagent Co. Ltd (Shanghai, China). Nafion (5 *wt.*%) was purchased from Sigma-Aldrich Chemical Reagent Co., Ltd. Commercial 20% Pt/C was acquired from Johnson Matthey Corporation. Deionized water (18.2 MΩ $cm^{-1}$) was employed throughout all experiments. All chemicals were of analytical reagent grade and used without further purification.

**Preparation of Au nanowires (NWs):** The ultrathin Au NWs were prepared according to our previous work.[1] In a typical synthesis, 3.0 mL of 0.50 M 1-naphthol ethanol solution was added into 3.0 mL of 0.05 M $HAuCl_4$ aqueous solution at 60 °C under water bath conditions. After aging for a few minutes (~ 2 min), the resultant product was collected by centrifugation of 9000 rpm for 3 min, washed with ethanol several times, and re-dispersed in ethanol.

**Preparation of Au@RuNi (also denoted as Au@$Ru_1Ni_2$) NWs:** For the synthesis of Au@RuNi NWs, 6.0 mg prepared Au NWs, 30 mg PVP, and 100 mg AA were added into the solvent of 10 mL EG in a 30 mL vial. After uniform dispersion by sonication, the vial was immersed in an oil bath held at 200 ℃ under magnetic stirring. The lid seals the reaction vial, creating a relatively closed system, thereby obviating the necessity for additional reflux apparatus. When the evaporated EG contacts the lid on the reaction vial, it condenses and flows back into the reaction system. Then, 7.5 mL 4.0 M $Ru(acac)_3$ EG solution and 7.5 mL 8.0 M $Ni(acac)_2$ EG solution were injected synchronously into the mixed solution in the vial using an injection pump at a rate of 3.75 mL $h^{-1}$. The detailed schematic diagram and digital photograph of the

experimental setup are depicted in Fig. S2. After the completion of the injection, the reaction system was kept at 200 °C for another 2 h. The produced Au@RuNi NWs were gathered by centrifugation of 16000 rpm for 6 min and washed multiple times with ethanol.

**Preparation of Au@$Ru_1Ni_1$ NWs and Au@$Ru_2Ni_1$ NWs:** The synthesis of Au@$Ru_1Ni_1$ and Au@$Ru_2Ni_1$ NWs were similar to that of Au@$Ru_1Ni_2$ NWs, except for substituting the 7.5 mL 8.0 M $Ru(acac)_3$ EG solution and 7.5 mL 4.0 M $Ni(acac)_2$ EG solution for 7.5 mL 4.0 M $Ru(acac)_3$ EG solution and 7.5 mL 4.0 M $Ni(acac)_2$ EG solution or 7.5 mL 4.0 M $Ru(acac)_3$ EG solution and 7.5 mL 8.0 M $Ni(acac)_2$ EG solution, respectively.

**Preparation of Au@Ru NWs and Au@Ni NWs:** The synthesis of Au@Ru and Au@Ni NWs were similar to that of Au@RuNi NWs, except for substituting the 7.5 mL 8.0 M $Ru(acac)_3$ EG solution and 7.5 mL 4.0 M $Ni(acac)_2$ EG solution for only 7.5 mL 8.0 M $Ru(acac)_3$ EG solution or only 7.5 mL 4.0 M $Ni(acac)_2$ EG, respectively.

**Preparation of RuNi alloy:** The synthesis RuNi alloy were similar to that of Au@RuNi NWs, except for adding the Au NWs.

**Characterizations:** Transmission electron microscopy (TEM), high-resolution TEM (HRTEM), high-angle annular dark-field scanning transmission electron microscopy (HAADF-STEM), and energy dispersive X-ray (EDX) elemental mapping measurements were made on a JEOL JEM-2100F transmission electron microscopy operated at an accelerating voltage of 200 kV. The crystallinity of the samples was determined by recording X-ray diffraction (XRD) patterns on a Model D/max-rC X-ray diffractometer using Cu Kα radiation source (λ = 1.5406 Å) and operating at 40 kV and 100 mA. X-ray photoelectron spectroscopy (XPS) measurements were performed with a Thermo VG Scientific ESCALAB 250 spectrometer with a monochromatic Al Kα X-ray source. The binding energy was calibrated by means of the C1s peak energy of 284.6 eV.

**Electrochemical measurements:** All electrochemical measurements were performed in a standard three-electrode electrochemical cell at ambient temperture using a CHI 760E workstation (CH Instruments, Shanghai, Chenhua Co., Ltd.). A graphite rod serves as auxiliary electrode and a saturated calomel electrode (SCE) works as reference electrode. For the preparation of catalyst inks, 2.0 mg prepared NWs or commercial Pt black and 2.0 mg Vulcan XC-72 carbon were well dispersed in 1.0 mL mixed solvent consisting of 0.60 mL ethanol and 0.30 mL $H_2O$, and 0.10 mL Nafion solution (5 *wt.*%) with the following sufficient sonication. Then, the glassy carbon electrode (*d*=3 mm) loaded with 10 μL of the mixed catalyst ink was used as the working electrode. Electrochemical HER was investigated in $N_2$-saturated 1.0 M KOH solution with a sweeping rate of 5 mV $s^{-1}$. All the polarization curves were obtained by iR compensation in this work, which was performed in CHI 760E workstation via automatically calculating the resistance. All electrode potentials were quoted versus reversible hydrogen electrodes (RHE). We conducted the RHE calibration with reference to a method in the literature, while in our electrochemical test system of 1.0 M KOH, $E$(RHE) = $E$(SCE) + 1.071 V.[2] Turnover frequency (TOF) was calculated with using following equation: $TOF = jA/nFN$, where $j$ is the current density under overpotential $\eta$ = 50 mV, $A$ is the geometric area of the working electrode, $n$ is the electron transferred number in the HER reaction ion (*i.e.* 2), $F$ is the Faraday constant of 96485.3 C $mol^{-1}$, and $N$ is the number of active sites (mol) calculated with the total mass loading. Electrochemical double-layer capacitance ($C_{dl}$) was calculated from the CV curves tested in a non-Faradic region under different scan rates from 40 to 200 mV $s^{-1}$. The electrochemically active surface areas (ECSA) is calculated by assuming a standard value of 60 μF $cm^{-2}$: ECSA= $C_{dl}$/60. Electrochemical impedance spectroscopy (EIS) was tested over a frequency range of 100 kHz-0.1 Hz. The accelerated durability test (ADT) of CVs is performed between the potential range from -0.05 V to 0.05 V vs. RHE for 10,000 cycles with a scan rate of 100 mV $s^{-1}$. The long-term durability was recorded by chronopotentiometry measurement at 10 mA $cm^{-2}$ for 25 h.

**Part II: Figures and Tables**

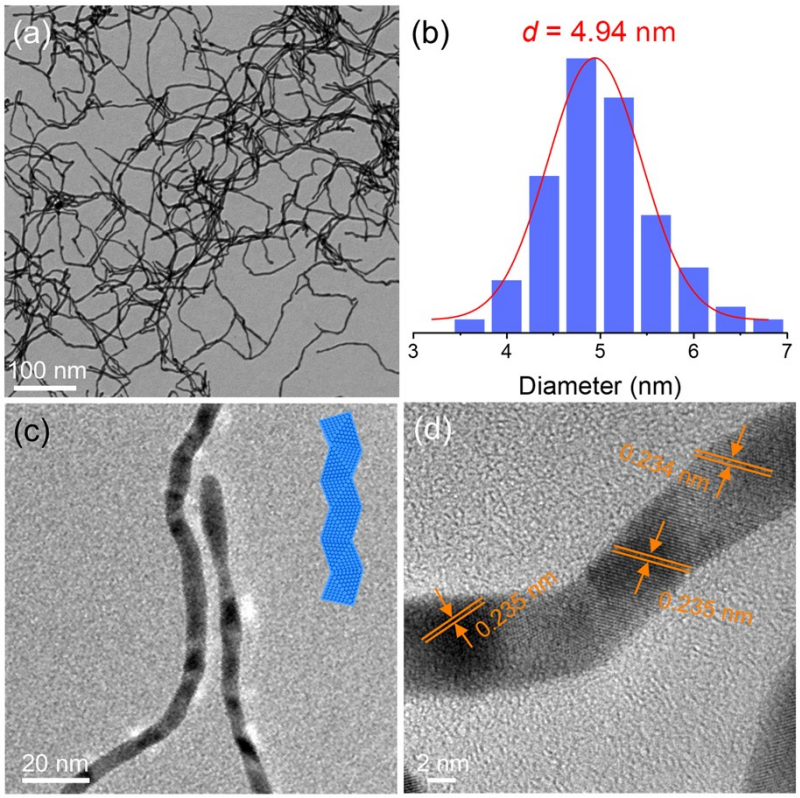


**Fig. S1** (a, c) TEM image, (c) particle-size distribution histogram, and (d) HRTEM images of Au NWs.

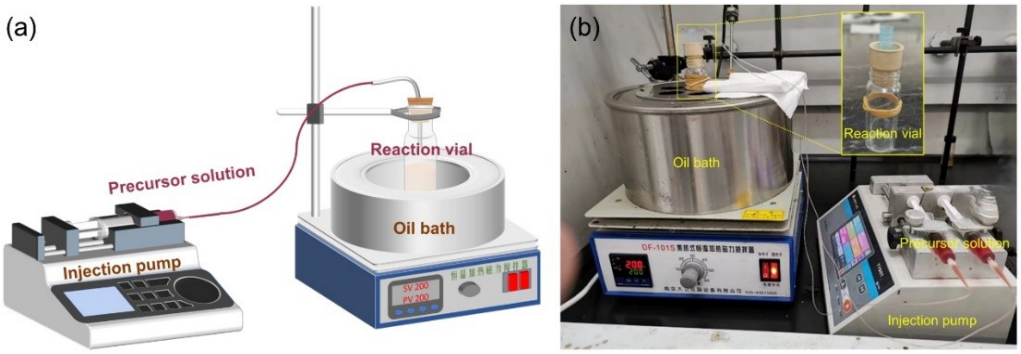


**Fig. S2** (a) The schematic diagram and (b) the digital photo of the experimental set-up of Au@RuNi NWs.

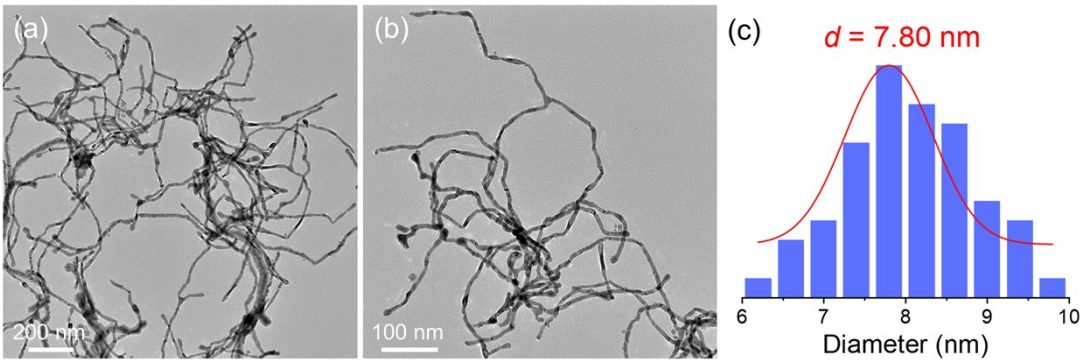


**Fig. S3** (a) TEM image, (b) HRTEM image, and (c) particle-size distribution histogram of Au@RuNi NWs.

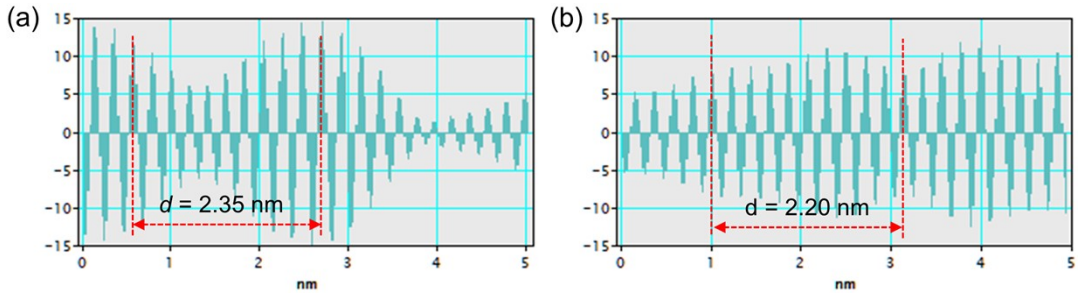


**Fig. S4** Profiles of the inverse fast Fourier transformation (IFFT) of (a) Au lattice taken from orange rectangular region and (b) Ru lattice taken from cyan rectangular region in Fig. 1e.

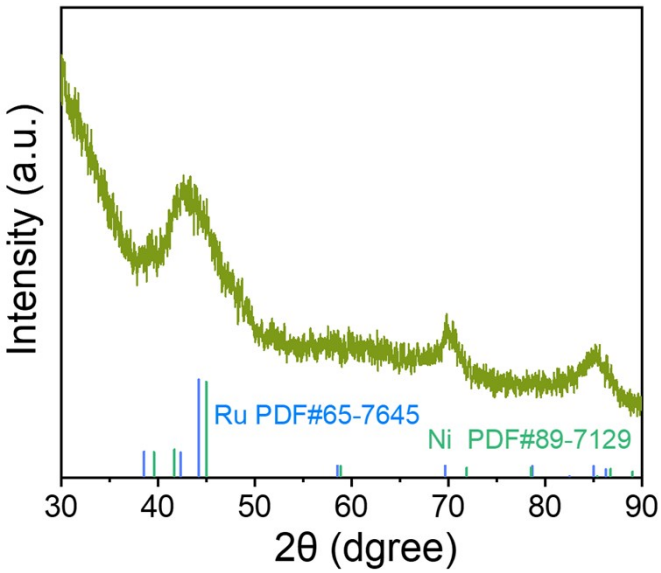


**Fig. S5** XRD pattern of the RuNi alloy.

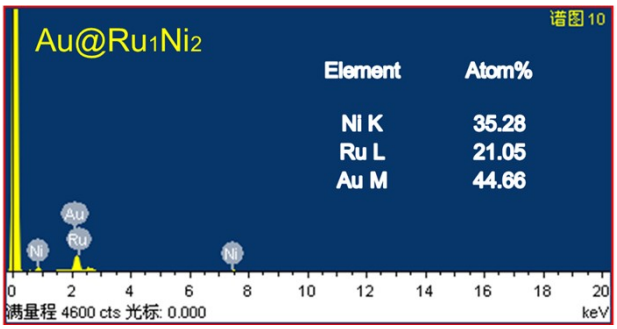


**Fig. S6** EDX spectrum of Au@RuNi (also denoted as Au@$Ru_1Ni_2$) NWs.

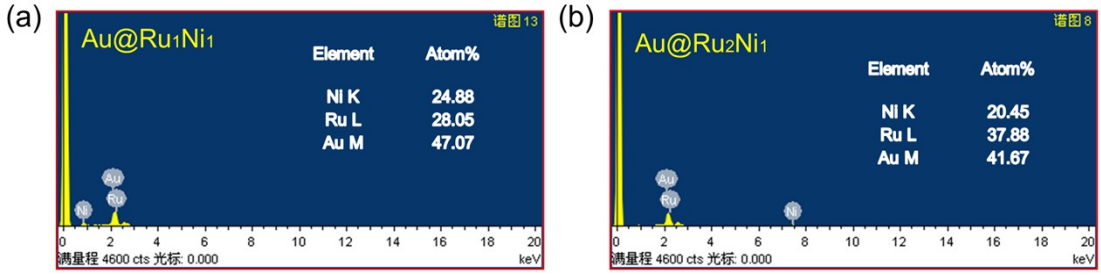


**Fig. S7** EDX spectra of (a) Au@$Ru_1Ni_1$ NWs and (b) Au@$Ru_2Ni_1$ NWs.

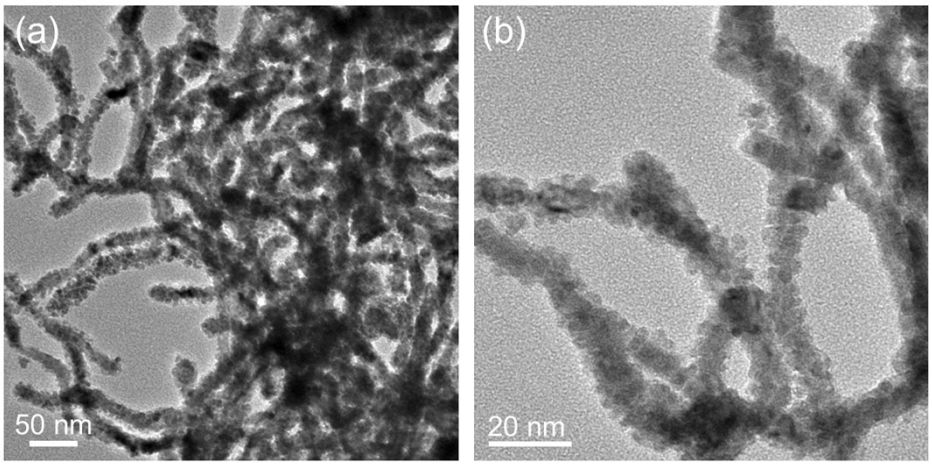


**Fig. S8** (a-b) TEM images of Au@Ru NWs.

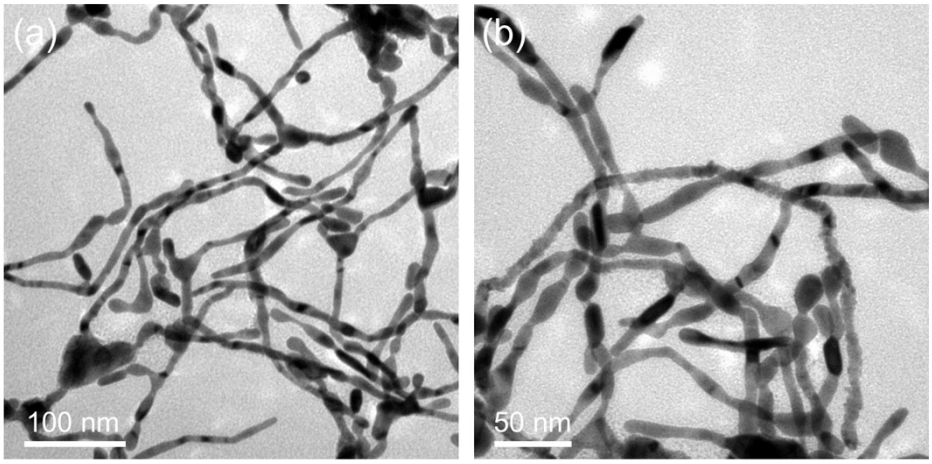


**Fig. S9** (a-b) TEM images of Au@Ni NWs.

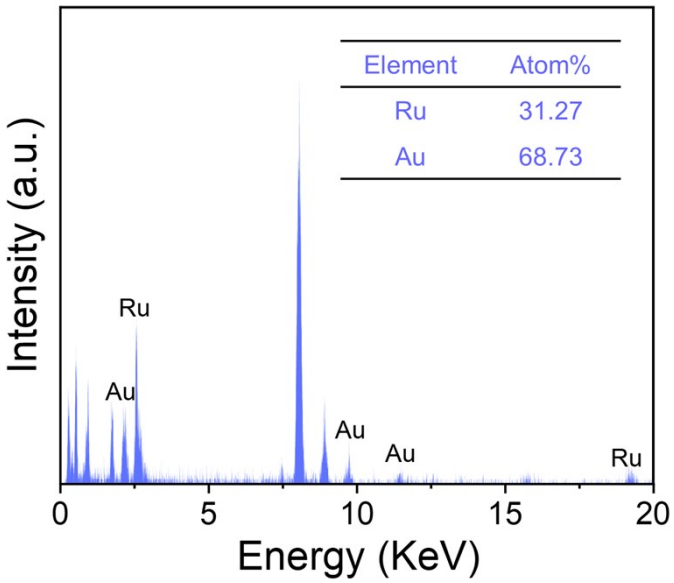


**Fig. S10** EDX spectrum of Au@Ru NWs.

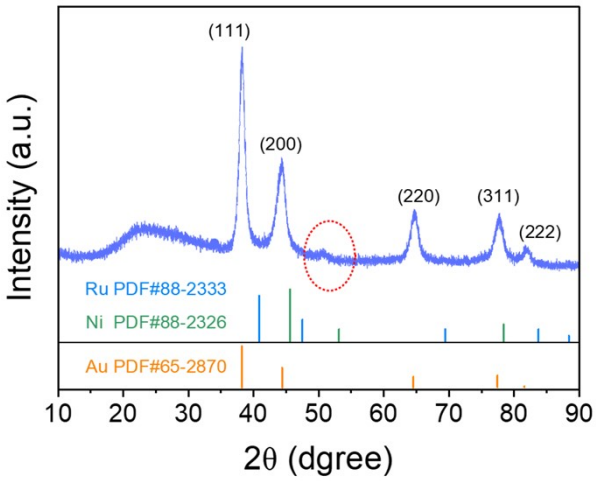


**Fig. S11** XRD pattern of Au@RuNi NWs.

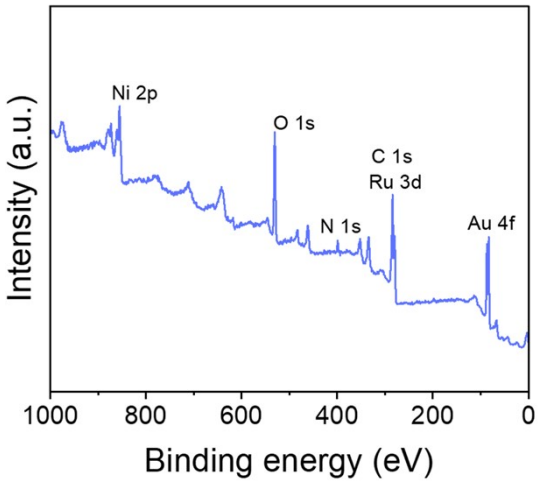


**Fig. S12** XPS survey scan spectrum of Au@RuNi NWs.

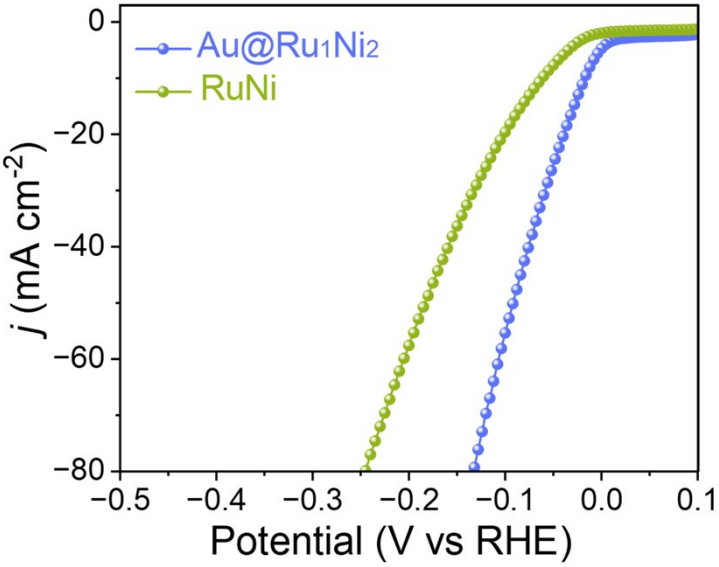


**Fig. S13** HER polarization curves of the Au@$Ru_1Ni_2$ NWs and RuNi alloy in $N_2$-saturated 1.0 M KOH solution.

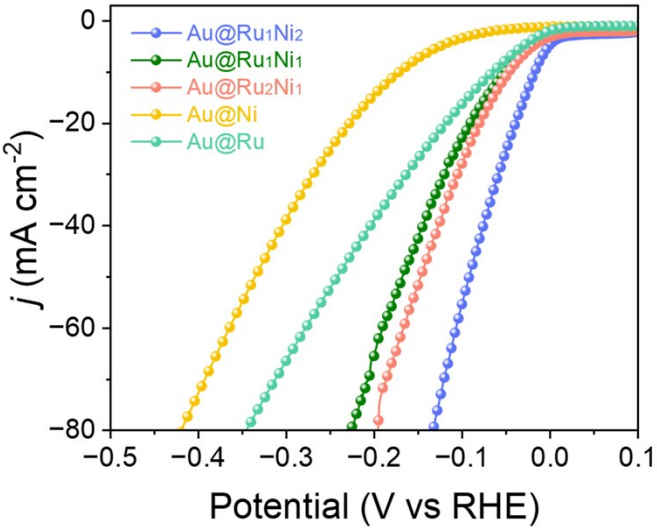


**Fig. S14** HER polarization curves of the Au@$Ru_xNi_y$ NWs with different Ru and Ni contents in $N_2$-saturated 1.0 M KOH solution.

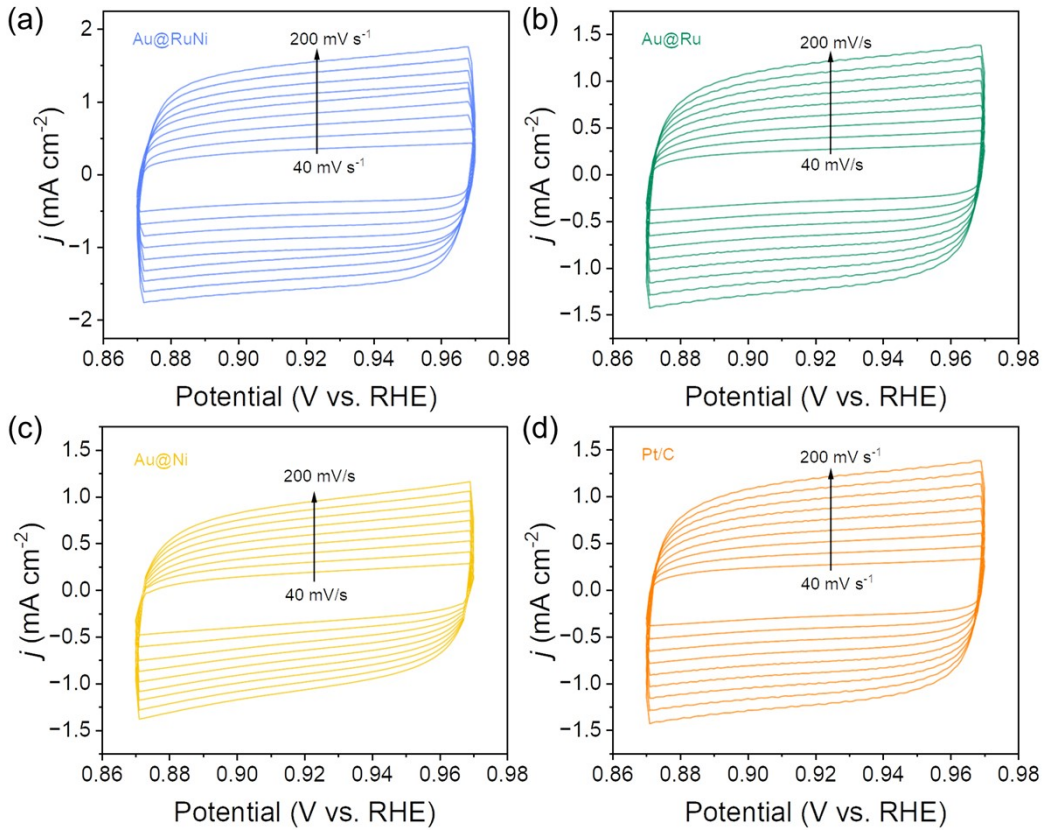


**Fig. S15** CV plots of (a) Au@RuNi NWs, (b) Au@Ru NWs, (c) Au@Ni NWs, and (d) commercial Pt/C with varying scan rates from 40 to 200 mV $s^{-1}$ in 1.0 M KOH.

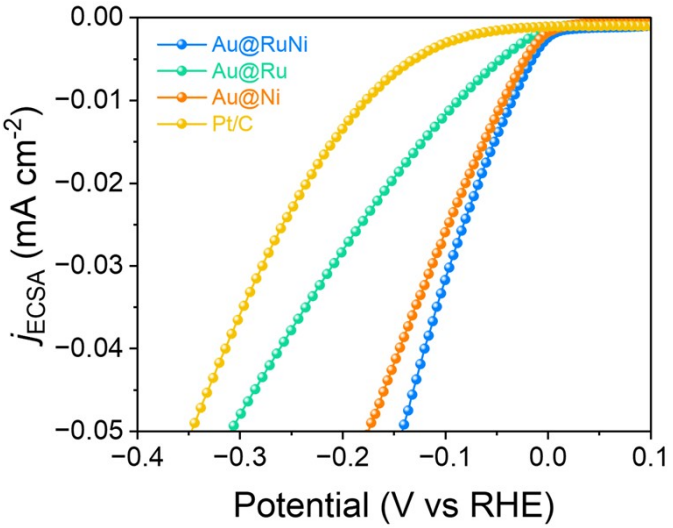


**Fig. S16** The ECSA-normalized HER polarization curves of the catalysts in $N_2$-saturated 1.0 M KOH.

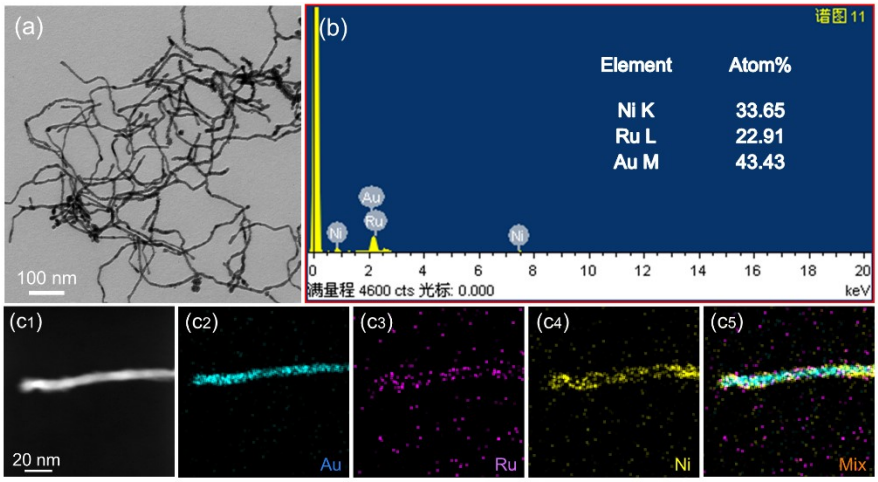


**Fig. S17** (a) TEM image, (b) EDX spectrum, (c) HAADF-STEM image and corresponding elemental mapping images of Au@RuNi NWs after the stability test.

**Table S1** Comparison of the HER activity with other reported noble metal-based electrocatalysts in 1.0 M KOH.

| Catalysts | $\eta_{10}$ (mV) | Tafel Slope (mV dec$^{-1}$) | References |
|---|---|---|---|
| **Au@RuNi** | **19** | **32.63** | **This work** |
| Ni@$Ni_2P$-Ru | 31 | 41 | J. Am. Chem. Soc. **2018**, 140, 8, 2731. |
| $RuP_2$@NPC | 52 | 69 | Angew. Chem. Int. Ed. **2017**, 56, 11559. |
| $Ru_2P$ | 64 | 36.7 | ChemSusChem **201**8, 11, 2724. |
| RuNi NPNWs | 69 | 73 | Int. J. Hydrogen Energy **2022**, 47, 31330. |
| S-RuP@NPSC | 92 | 90.23 | Adv. Sci. **2020**, 7, 2001526. |
| Ru SAs-$Ni_2P$ | 57 | 75 | Nano Energy **2021**, 80, 105467. |
| M-Co NPs@Ru SAs/NC | 34 | 55 | Small **2021**, 17, 2105231. |
| Ru@WNO-C | 24 | 39.7 | Nano Energy **2021**, 80, 105531. |
| $Ru_1Ni_1$-NCNFs | 35 | 30 | Adv. Sci. **2020,** 7, 1901833. |
| Ru-Cu@C-2 | 20 | 37 | Sci. Bull. **2021**, 66, 257. |
| $RuO_2$/NiO/NF | 22 | 31.7 | Small **2018**, 14, 1704073. |
| Mo-$RuCOO_x$ | 41 | 24.3 | Adv. Funct. Mater. **2023**, 2303073. |
| a/c-$RuCoMo_yO_x$/NF | 39 | 65.9 | Chem. Eng. J. **2023**, 469, 143993. |
| Ru@$MoO(S)_3$ | 30 | 29 | Nano Energy **2022,** 100, 107445. |
| CoRu–$MoS_2$ | 52 | 55 | Small **2020**, 16, 2000081. |
| Ru/$Co_4N$-$CoF_2$ | 53 | 144.1 | Chem. Eng. J. **2021**, 414, 128865. |
| $SrTi_{0.7}Ru_{0.3}O_{3-\delta}$ | 46 | 40 | Nat. Commun. **2020,** 11, 5657. |
| Ru-$Co_2P$/N-C/NF | 65 | 65 | Chem. Eng. J. **2021**, 408, 127308. |
| (Ru-Co)$O_x$ | 44.1 | 23.5 | Angew. Chem. Int. Ed. **2020**, 59, 17219. |
| $Ni_5P_4$-Ru | 123 | 56.7 | Adv. Mater. **2020**, 32, 1906972. |
| $Ni_2P$-$Fe_2P$-$Ru_2P$/NF | 78.6 | 37.9 | J. Mater. Chem. A, **2022**,10, 772. |
| ECM@Ru | 83 | 59 | Adv. Energy Mater. **2020**, 10, 2000882. |

**Table S2** Comparison of the overall water splitting performance of the Au@RuNi NWs // $RuO_2$ with other recently reported Ru-based catalysts in 1.0 M KOH solution.

| Catalysts | Potential @ 10 mA $cm^{-2}$ | References |
|---|---|---|
| **Au@RuNi NWs // $RuO_2$** | **1.50 V** | **This work** |
| 2% Ru-NCO // 2% Ru-NCO | 1.55 V | Chem. Eng. J. **2022**, 439, 135634. |
| Ru-G/CC // Ru-$H_2O$/CC-350 | 1.67 V | Appl. Catal. B: Environ. **2022**, 317, 121729. |
| P-Ru-CoNi-LDH // P-Ru-CoNi-LDH | 1.53 V | Small **2022**, 18, 2104323. |
| Ru-$NiSe_2$/NF // Ru-$NiSe_2$/NF | 1.54 V | Small **2022**, 18, 2105305 |
| Ru-$VO_2$ // Ru-$VO_2$ | 1.54 V | Adv. Mater. **2024**, 36, 2310690 |
| NiRu@Fe/C@CNT // Ni-Ru@Fe/C@CNT | 1.54 V | Chem. Eng. J. **2022**, 424, 130416 |
| CoVRu LDH // CoVRu LDH | 1.52 V | Chem. Eng. J. **2023**, 452, 139151 |
| Ru/$RuO_2$@NCS // Ru/$RuO_2$@NCS | 1.51 V | InfoMat **2022**, 4, e12326 |
| Co-Ru/NCN CC // Co-Ru@$RuO_x$/NCN CC | 1.56 V | J. Energy Chem. **2023**, 87, 286 |
| Ru-$Ru_2P$ // NiFe-LDH/CNTs | 1.53 V | Small **2023**, 19, 2208045 |
| Ru@$MoO(S)_3$ // Ru@$MoO(S)_3$ | 1.53 V | Nano Energy **2022**, 100, 107445 |
| Ru-$NiCo_2O_4$ NSs // Ru-$NiCo_2O_4$ NSs | 1.60 V | Chinese Chem. Lett. **2022**, 33, 4930 |
| $RuO_2$ // NCPO-Ru NCs | 1.56V | ACS Nano **2022**, 16, 7993 |
| Ru-$Co_2P$@Ru-N-C // Ru-$Co_2P$@Ru-N-C | 1.56 V | Adv. Funct. Mater. **2024**, 2316709 |

## References


1 X. Jiang, X. Qiu, G. Fu, J. Sun, Z. Huang, D. Sun, L. Xu, J. Zhou and Y. Tang, Highly simple and rapid synthesis of ultrathin gold nanowires with (111)-dominant facets and enhanced electrocatalytic properties, *J. Mater. Chem. A*, 2018, **6**, 17682-17687.

2 Y. Y. Liang, Y. G. Li, H. L. Wang, J. G. Zhou, J. Wang, T. Regier and H. J. Dai, $Co_3O_4$ nanocrystals on graphene as a synergistic catalyst for oxygen reduction reaction, *Nat. Mater.*, 2011, **10**, 780-786.